Routes to DNA Accessibility: Alternative Pathways for Nucleosome Unwinding

Daniel J. Schlingman, Andrew H. Mack, Masha Kamenetska Simon G.J. Mochrie and Lynne Regan

Supplementary Notes:

Materials and Methods:

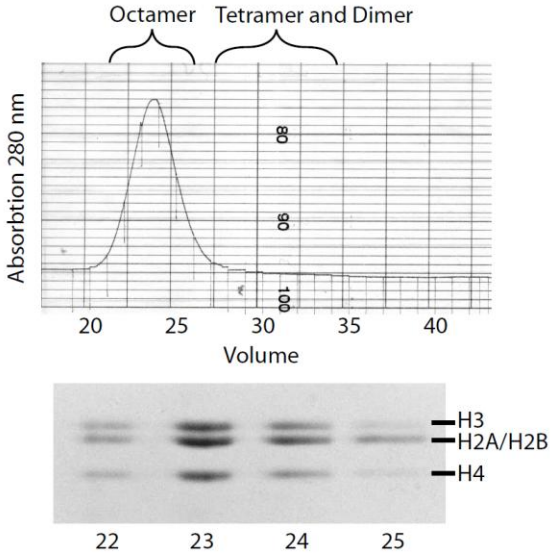

Figure S1: Formation of histone octamer. Octamer formed by dialysis from 6M gaunidine to 2M NaCl is separated from unincorporated dimer and tetramer on a size exclusion column. Octamer fractions were collected and run using SDS-PAGE.

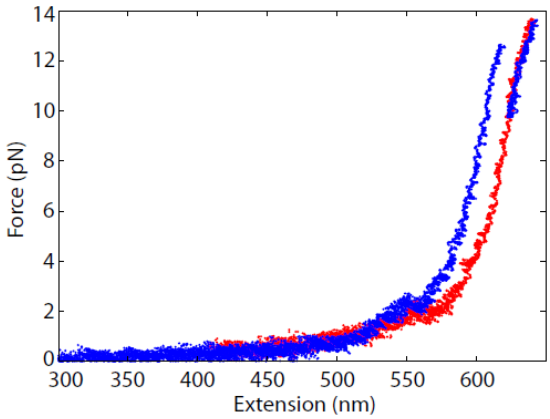

Figure S2: Example force versus extension trace of a nucleosome loaded onto a single repeat of the 601 nucleosome positioning sequence. Blue is pulling while red is relaxing. Around 2 pN, there is a step corresponding to the transition from state 2 to state 1. At ~13 pN, there is a transition from state 1 to a completely unwound form.

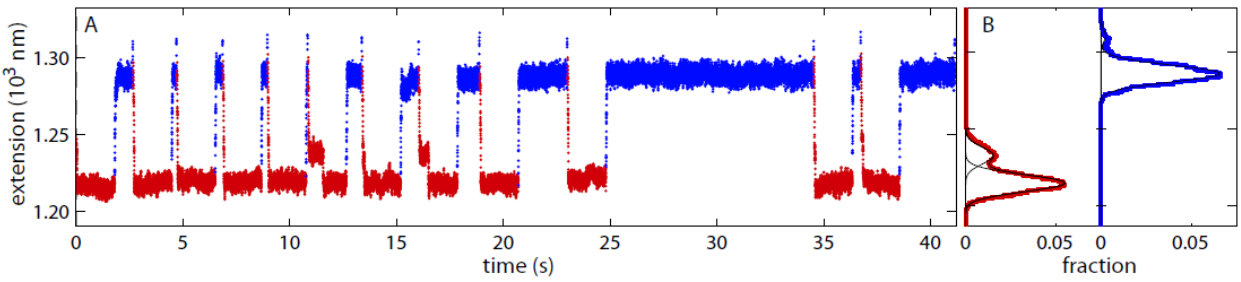

Figure S3: Example trace showing nucleosome unwinding and rewinding using the molecular yo-yo method. *(A)* Nucleosome unwinding at 12.2 pN is shown in blue. Nucleosome rewinding at 3.8 is shown in red. To unwind a nucleosome, the force is first increased to the desired value (this increase in force causes a corresponding increase in extension of ~75 nm because of the additional stretching of the DNA handles). The nucleosome is then held at a constant force. When the nucleosome unwinds, the extension increases by ~25 nm as seen at the end of each blue trace. The force is then lowered causing a decrease in extension of ~75 nm as a result of the reduced tension in the DNA handles. When the nucleosome rewinds, there is a further decrease in extension of ~25 nm. *(B)* Histogram of the extensions, shown in A, for unwinding (blue) and rewinding (red). The high force and low force histograms are fit with two Gaussians. The lower extension peak corresponds to the extension of the wound nucleosome and the higher extension peak corresponds to the extension of the unwound nucleosome. The extension difference in peak height corresponds to the step size of the nucleosome unwinding/rewinding event.

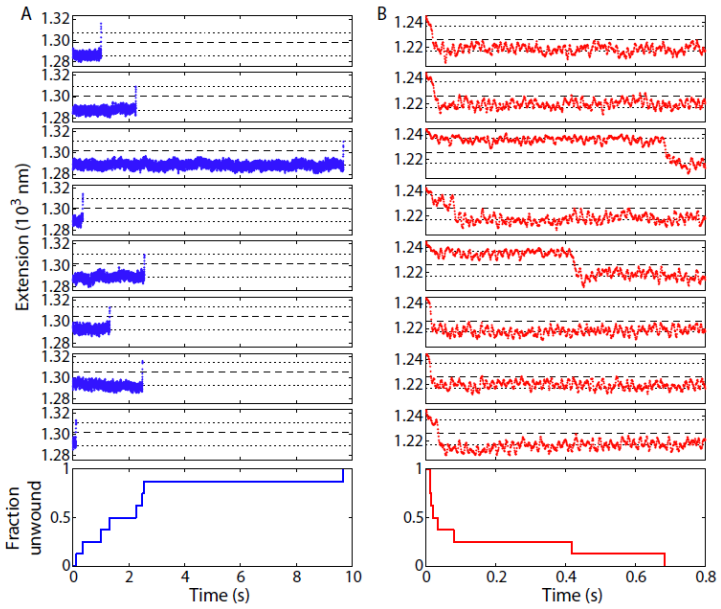

Figure S4: Individual example unwinding/rewinding traces. *(A)* Eight extension versus time traces of individual unwinding events at a force of 12.2 pN. The lower dotted line represents the wound state and corresponds to the mean of 40 points measured before the jump. The upper dotted line represents the extension of the unwound state. The dashed line is 12 nm from the lower dotted line, and represents the threshold extension for jump detection in each trace. The time measured for each unwinding event is added to a cumulative distribution shown as a solid blue line in the bottom panel. *(B)* Same as A for rewinding at 3.8 pN.

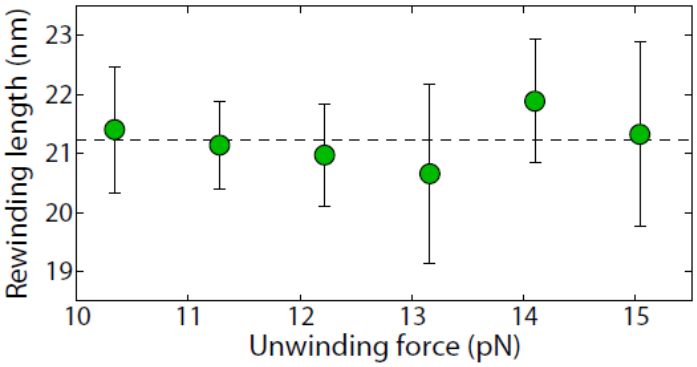

Figure S5: Step-size of nucleosome rewinding at 3.8 pN after being unwound at different forces.

Probability Distributions:

The cumulative lifetime distributions presented and discussed in the main text are simply and directly related to our measurements. However, a quantitative statistical comparison between these measurements and model lifetime distributions is facilitated by focusing on the distribution of lifetimes, i.e. the number of lifetime measurements within time bins. Therefore, we created a histogram of the measured unwinding and rewinding times with logarithmically-spaced bins. A key advantage of employing these distributions for statistical analysis is that the numbers of counts in different bins are uncorrelated with each other, allowing for straightforward application of the χ^2 goodness-of-fit test.

Histograms corresponding to the cumulative rewinding lifetime distributions shown in the main text in Fig. 2c, 3a-b, and Fig. 4a, are shown in Fig. S6, Fig. S7, and Fig. S8. The error bars in these figures correspond to one-standard deviation errors, determined from counting statistics.

Figure S6 shows the histograms of rewinding times at 3.8 pN after unwinding at (a) 10.3 , (b) 11.3, (c) 12.2, (d) 13.2, and (e) 14.1 pN, corresponding to the cumulative lifetime distributions shown in Fig. 2(c). For each histogram, a single exponential lifetime distribution with the maximum likelihood rate is shown as the gray, dashed curve, while a two-exponential model, corresponding to two unwound states, is shown as a solid, colored curve. The two rates in the two-exponential model were set equal to the maximum likelihood rates from the single exponential model at 10.3 and 14.1 pN. The relative amplitude of the two exponentials was determined by maximum likelihood. Thus, both models each have one free parameter. For forces of 10.3 (a), 11.3 (b), and 14.1 pN (e), the single exponential model and the two-exponential model are nearly coincident, showing that, at each of these conditions, the distribution of rewinding times approaches a single exponential. However, for rewinding at 3.8 pN after unwinding at 12.2 and 13.1 pN, the single exponential model and the two-exponential model differ significantly with the two-exponential model providing a noticeably superior description of the experimental distribution of rewinding times.

Fig. S7 shows the histogram of rewinding times at three forces for nucleosomes unwound at 14.1 (a-c) or 10.3 (d-f) pN, corresponding to the data in Fig. 3a-b. Overlaid on each plot is a single exponential lifetime distribution with a rate determined by maximum likelihood. As can be seen, for the majority of bins, the measured number of counts lies within one standard deviation of the number of counts predicted on the basis of the single-exponential model.

Figure S8 shows a similar analysis for the unwinding lifetime distribution at 12.3 pN for salt concentrations of 50, 100, 150, and 200 mM, corresponding to the data shown in Fig. 4c. Single exponentials with maximum likelihood rates show good agreement with the measured distributions, similar to Fig. S7.

To quantify the goodness of fit in each case, we evaluated the reduced χ^2 values (henceforth referred to simply as the χ^2 values) for each rewinding lifetime histogram and each model tested, where

$$\chi^2 = \frac{1}{n-1}\sum_{i=1}^{n}\frac{[c_i - m_i]^2}{\sigma_i^2}, \qquad \text{Eq. S1}$$

where c is the measured number of counts in the i'th bin, m is the predicted number of counts for the i'th bin and σ_i is the predicted variance for the i'th bin. The sum is taken over the n bins with nonzero counts. Each χ^2 value and the probability of realizing that value or a larger value of χ^2 are presented in Table S1 or Table S2.
Table S1 gives the χ^2 values and probabilities for the rewinding distributions measured at 3.8 pN after unwinding at 10.3, 11.3, 12.2, 13.2, and 14.1 pN, and fitted to both the single exponential model and the two-exponential model. Table S2 gives the χ^2 values and corresponding probabilities for rewinding distributions measured at 1.9, 2.4, 2.8, 3.3, 3.8, and 4.7 pN after unwinding at 10.3 pN and measured at 3.8, 4.2, 4.7, 5.2, and 5.6 pN after unwinding at 14.1 pN, fitted to the single exponential model.

If we define a probability of 5% or less to be an unacceptable fit, then there are two unacceptable fits. Specifically, the single exponential description of the rewinding lifetime distributions measured after unwinding at 12.2 and at 13.2 pN provide an unacceptable fit. By contrast, the two-exponential model does provide an acceptable fit to these data.

Lastly, Table S3 summarizes the χ^2 values for a similar analysis of the measured unwinding lifetime distributions, fitted to a single-exponential model, corresponding to the unwinding rates summarized in Fig. 4c. The single exponential model provides an acceptable fit to the unwinding lifetime distributions in every case.

In summary, this analysis clearly demonstrates that all of our measurements of unwinding lifetime distributions and all but two of our measurements of rewinding lifetime distributions are in agreement with a single exponential model. Importantly, however, our analysis also shows that out measurements of the rewinding lifetime distributions after unwinding at 12.2 and 13.1 pN are not in agreement with a single exponential model, but instead are in agreement with a two-exponential model corresponding to the existence of two unwound states.

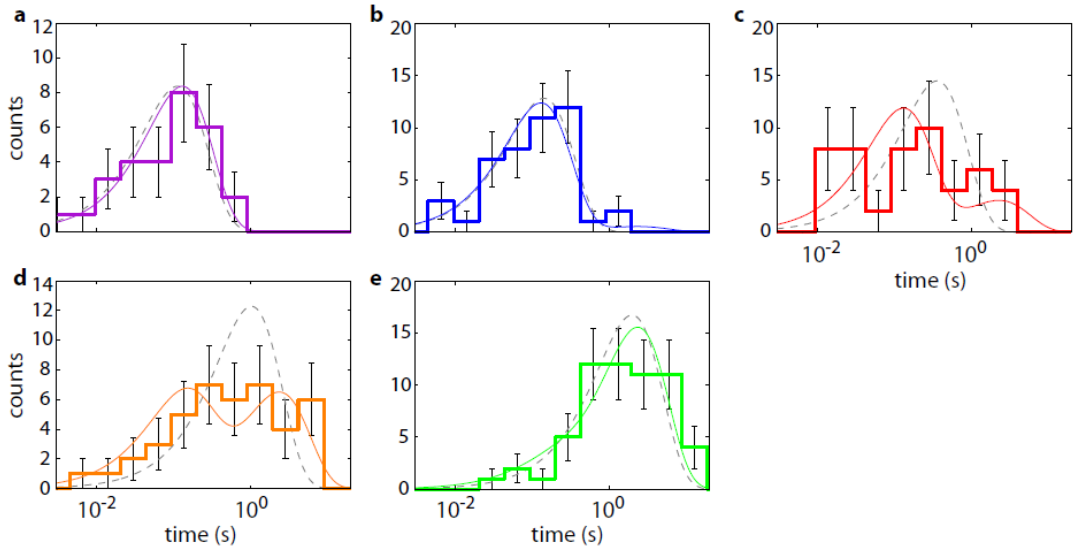

Supplementary Figure 6. Comparison of single exponential model and two unwound state model to rewinding data. Histogram of rewinding times at 3.8 pN after unwinding at **a,** 10.3 (purple), **b,** 11.3 (blue), **c,** 12.2 (red), **d,** 13.2 (orange), and **e,** 14.1 pN (green). In all panels, gray dashed lines are a single exponential with the maximum likelihood rate. Solid, colored lines show the fit of a two unwound state model, equation S4, described in text. Errors bars correspond to one standard deviation, predicted on the basis of the experimental distribution's counting statistics.

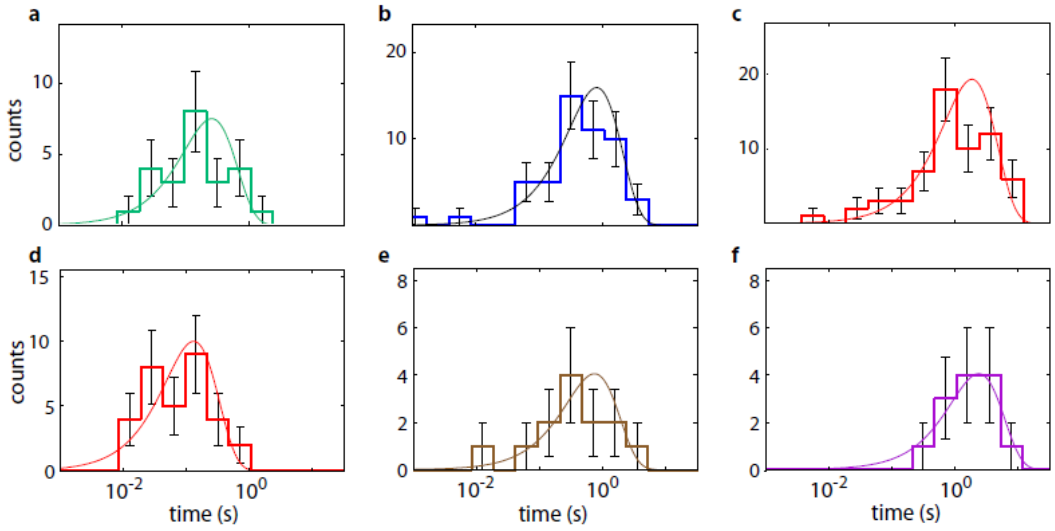

Supplementary Figure 7. Histograms of rewinding times follow an exponential distribution. Histogram of nucleosome rewinding plotted at **a,** 2.8 (teal), **b,** 3.3 (blue), and **c,** 3.8 (red) pN after unwinding at 14.1 pN. and **d,** 3.8 (red), **e,** 4.2 (brown), and **f,** 4.7 (purple) pN after unwinding at 10.3 pN. Solid lines are a single exponential with the maximum likelihood rate. Errors represent one standard deviation predicted from experimental distribution's counting statistics.

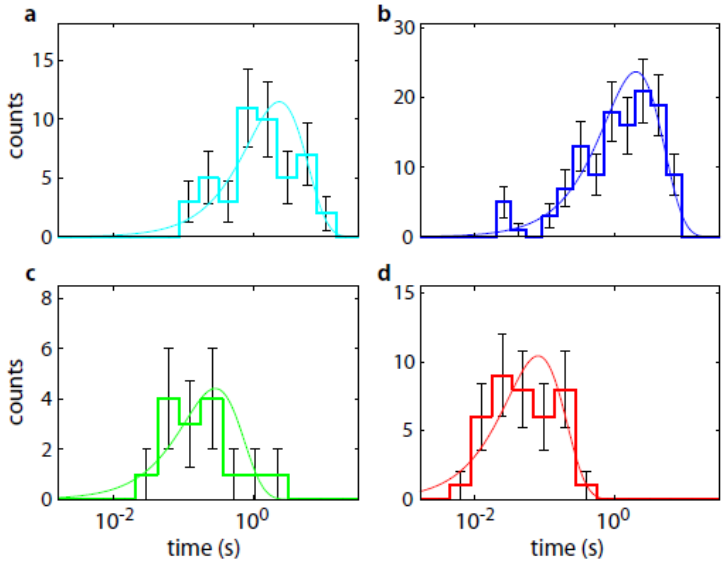

Supplementary Figure 8. Histogram of unwinding times at 12.2 pN for **a,** 50, **b,** 100, **c,** 150 and **d,** 200 mM NaCl. Solid lines are a single exponential with the maximum likelihood rate. Errors represent one standard deviation predicted from experimental distribution's counting statistics.

Supplementary Table 1. Goodness of fit, χ^2, values for rewinding time distributions at 3.8 pN shown in Fig. S2 and in Fig. 2c. Failing values corresponding to a probability less than 5% are shown in bold red. We note that for both forces at which significant state mixing is predicted, a two unwound state model gives a passing χ^2 whereas a single exponential fails to satisfactorily fit the data.

	χ^2	Probability	χ^2	Probability
Unwinding Force	Goodness-of-fit (χ^2) for the single exponential model		Goodness-of-fit (χ^2) for the two exponential model (Eq. S4)	
10.3 pN	0.3	97%	0.4	92%
11.3 pN	1.2	29%	1.3	24%
12.2 pN	**4.9**	**0.0005%**	1.6	12%
13.2 pN	**2.3**	**0.8%**	0.3	99%
14.1 pN	0.8	61%	0.7	71%

Supplementary Table 2. Goodness of fit, χ^2, test to single exponential for rewinding distributions measured at 10.3 and 14.1 pN.

	Goodness-of-fit (χ^2) for rewinding after unwinding at 10.3 pN		Goodness-of-fit (χ^2) for rewinding after unwinding at 14.1 pN	
Force	χ^2	Probability	χ^2	Probability
1.9 pN	1.8	14%		
2.4 pN	0.9	51%		
2.8 pN	0.9	51%		
3.3 pN	0.8	60%		
3.8 pN	1.5	17%	1.3	26%
4.2 pN			0.9	51%
4.7 pN	1.0	39%	0.1	99%
5.2 pN			1.3	25%
5.6 pN			0.9	41%

Supplementary Table 3. Goodness of fit χ^2 test to single exponential for unwinding distributions measured at different salt concentration and forces.

	Goodness-of-fit (χ^2) for the unwinding lifetime distribution at 50 mM NaCl		Goodness-of-fit (χ^2) for the unwinding lifetime distribution at 100 mM NaCl		Goodness-of-fit (χ^2) for the unwinding lifetime distribution at 150 mM NaCl		Goodness-of-fit (χ^2) for the unwinding lifetime distribution at 200 mM NaCl	
Force	χ^2	Prob.	χ^2	Prob.	χ^2	Prob.	χ^2	Prob.
7.5 pN	1.3	27%					0.8	45%
8.5 pN	2.3	6%	1.7	14%	0.8	44%	0.2	90%
9.4 pN	1.9	8%	0.6	66%	1.1	33%	1.7	18%
10.3 pN	0.7	67%	0.8	59%	1.4	22%	0.4	75%
11.3 pN	1.4	22%	1.4	21%	0.3	91%	1.6	18%
12.2 pN	1.3	25%	1.8	7%	0.2	94%	0.1	96%
13.2 pN	0.1	100%	0.6	76%	0.5	61%		
14.1 pN	0.1	100%	0.7	67%				
14.6 pN	0.1	100%						
15.0 pN	1.2	31%	1.4	22%				

Supplementary Table 4. Fit parameters used in Fig. 3 following Eq. S1-3. Errors are one standard deviation. Fits were determined using Matlab commands `nlinfit` with weighting and `nlparci`.

[NaCl] (mM)	C_L (s^{-1})	C_H (s^{-1})	$k_{plateau}$ (s^{-1})	x_H (pN^{-1})	x_L (pN^{-1})
50	$(2\pm2)\times10^{-7}$	$(2\pm3)\times10^{-13}$	0.4±0.4	1.9±0.2	1.5±0.2
100	$(2\pm2)\times10^{-7}$	$(2\pm3)\times10^{-12}$	0.5±0.5	1.9±0.2	1.5±0.2
150	$(2\pm3)\times10^{-7}$	$(3\pm4)\times10^{-11}$	0.3±0.3	1.9±0.2	1.5±0.2
200	$(2\pm2)\times10^{-7}$	$(5\pm5)\times10^{-10}$	0.5±0.6	1.9±0.2	1.5±0.2

Two unwound state model of nucleosome unwinding

A prediction of the two unwound state unwinding model, which directly follows from the above description of unwinding rates $k_{1\to A}$ and $k_{1\to 0}$, is that unwinding into either state A or state 0 are both possible for a range of unwinding forces. The probability of undergoing an unwinding transition from state 1 into state 0 is $P_0=k_{1\to 0}/(k_{1\to 0}+k_{1\to A})$. Likewise, the state 1 to state A transition probability is therefore $1-P_0$. Using the fits shown in Fig. 3 for $k_{1\to 0}$ and $k_{1\to A}$, the prediction for the probability to unwind into state 0 is shown in Fig. 2b. The predicted values of P_0 show that the nucleosome can unwind into either state 0 or state A with high probability (greater than 20%) for forces of 12.2 and 13.1 pN. After unwinding at 12.2 or 13.1 pN, the nucleosome will be in either state 0 or state A, and, upon lowering the force, the rewinding rate will be either $k_{0\to 1}$ or $k_{A\to 1}$, respectively. This ability of the nucleosome to unwind into two different states, which then rewind with two different rates, will result in the measurement of a non-exponential distribution of rewinding times. We model the probability distribution of rewinding times at 3.8 pN, P_R, as the sum of two exponential distributions with rates $k_{0\to 1}$ and $k_{A\to 1}$, weighted by the probability to be in the respective state, namely,

$$P_R(t) = P_0\,[\exp(-k_{0\to 1}t)] + (1-P_0)[\exp(-k_{A\to 1}t)]. \qquad \text{Eq. S2.}$$

We determine $k_{0\to 1}$ from rewinding times at 3.8 pN after unwinding at 10.3 pN, where state 0 unwinding is dominant (P_0 = 99.6%, using prediction shown in Fig. 2). Similarly, we determine $k_{A\to 1}$ from rewinding times measured after unwinding at 14.1 pN, where state A unwinding is predicted to dominate ($1-P_0$ = 93.0%). The probability of measuring a particular set of rewinding times, t_n, for a value of P_0 is given by P_P

$$P_P(P_0) = \prod_{n=1}^{N} P_R(t_n) \Big/ \int_{P_{0=0}}^{P_{0=1}} \prod_{n=1}^{N} P_R(t_n)\,dP_0\,. \qquad \text{Eq. S3}$$

For the rewinding distributions at 3.8 pN after unwinding at a range of forces we determine the value of P_0 maximizing the probability P_P for the measured rewinding times, t_n, using the values of $k_{A\to 1}$ and $k_{0\to 1}$ determined previously. The cumulative distribution fits shown in Fig. 2c use this maximum likelihood value of P_0 and constant $k_{A\to 1}$ and $k_{0\to 1}$, and show good agreement with the measured distribution of times. Additionally, the determined values of P_0, shown in Fig. 2b, show good agreement with predictions from fits to the unwinding rates. The error bars shown in Fig. 2b correspond to one standard deviation calculated from the probability distribution of P_P for the set of measured times t_n at each force.

Maximum likelihood unwinding rate for different numbers of nucleosomes

The number of nucleosomes on the DNA at any given time affects the observed rate of unwinding. To correctly account for the number of nucleosomes in the determination of the single-nucleosome unwinding rate, we measure the number of nucleosomes on the DNA and use this number to calculate the single-nucleosome rate accordingly. Consider the probability P that one nucleosome unwinds in time dt after a waiting time t from an array of N nucleosomes.

$$P = Nke^{-Nkt}dt \qquad \text{Eq. S4}$$

For a total of A nucleosome unwinding events, when event i occurs at time t_i from an array of N_i nucleosomes, the maximum likelihood value of the single nucleosome unwinding rate is found by setting to zero the derivative of $\ln(P_{total}) = \sum ln(P_i)$ with respect to k:

$$\frac{dln(P_{total})}{dk} = \frac{1}{k}\sum_{i=1}^{A} -N_i t_i = 0 \qquad \text{Eq. S5}$$

Solving Eq. S5, we find that the maximum likelihood single-nucleosome unwinding rate is

$$k = \frac{A}{N_1 t_1 + N_2 t_2 \ldots N_A t_A} \quad . \qquad \text{Eq. S6}$$